

This document is confidential and is proprietary to the American Chemical Society and its authors. Do not copy or disclose without written permission. If you have received this item in error, notify the sender and delete all copies.

Exceptionally Fast Ion Diffusion in Block Copolymer-Based Porous Carbon Fibers

Journal:	<i>ACS Applied Materials & Interfaces</i>
Manuscript ID	am-2022-12755u
Manuscript Type:	Article
Date Submitted by the Author:	17-Jul-2022
Complete List of Authors:	Elliott, John; Virginia Polytechnic Institute and State University Osti, Naresh; Oak Ridge National Laboratory, Neutron Scattering Division Tyagi, Madhusudan; NIST Center for Neutron Research, Mamontov, Eugene; Oak Ridge National Laboratory, Neutron Scattering Science Division Liu, Lifeng; International Iberian Nanotechnology Laboratory, Quantum Materials, Science and Technology Serrano, Joel; Virginia Polytechnic Institute and State University, Chemistry Cao, Ke; Virginia Polytechnic Institute and State University, Macromolecules Innovations Institute Liu, Guoliang; Virginia Polytechnic Institute and State University, Department of Chemistry

SCHOLARONE™
Manuscripts

Exceptionally Fast Ion Diffusion in Block Copolymer-Based Porous Carbon Fibers

John P. Elliott^a, Naresh C. Osti^{b}, Madhusudan Tyagi^{c,d}, Eugene Mamontov^b, Lifeng Liu^e, Joel M. Serrano^a, Ke Cao^f, Guoliang Liu^{a,f*}*

^a Department of Chemistry, Virginia Tech, Blacksburg, VA 24061, United States

^b Neutron Scattering Division, Oak Ridge National Laboratory, PO BOX 2008 MS6455, Oak Ridge, TN 37831, United States

^c NIST Center for Neutron Research, National Institute of Standards and Technology, Gaithersburg, Maryland 20899, United States

^d Department of Materials Science, University of Maryland, College Park, Maryland 20742, United States

^e International Iberian Nanotechnology Laboratory (INL), Avenida Mestre José Veiga, 4715-330 Braga, Portugal

^f Macromolecules Innovation Institute, Virginia Tech, Blacksburg, VA 24061, United States

Corresponding Author

* gliu1@vt.edu; ostinc@ornl.gov

Keywords: block copolymer, porous carbon fiber, quasielastic neutron scattering, ion diffusion, room temperature ionic liquid

ABSTRACT

1
2
3 Confined ionic liquids in hydrophilic porous media have disrupted lattices and can be divided into
4 two layers: An immobile ion layer adheres to the pore surfaces and an inner layer exhibits faster
5 mobility than the bulk. In this work, we report the first study of ionic liquids confined in block
6 copolymer-based porous carbon fibers (PCFs) synthesized from polyacrylonitrile-*block*-
7 polymethyl methacrylate (PAN-*b*-PMMA). The PCFs contain a network of unimodal mesopores
8 of 13.6 nm in diameter and contain more hydrophilic surface functional groups than previously
9 studied porous carbon. Elastic neutron scattering shows no freezing point for 1-butyl-3-
10 methylimidazolium tetrafluoroborate ([BMIM]BF₄) confined in PCFs down to 20 K. Quasi-elastic
11 neutron scattering (QENS) is used to measure the diffusion of [BMIM]BF₄ confined in PCFs,
12 which, surprisingly, is seven-fold faster than in the bulk. The unprecedentedly high ion diffusion
13 remarks that PCFs hold exceptional potential for use in electrochemical catalysis, energy
14 conversion, and storage.

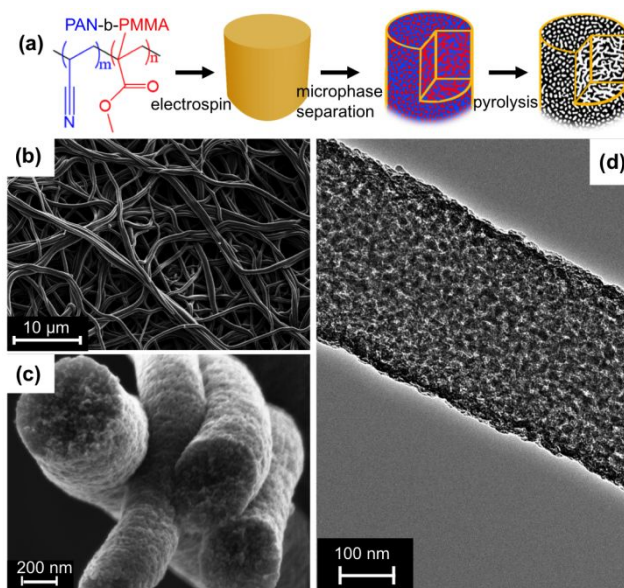
31 32 **1. Introduction**

33
34
35 Fast diffusion is crucial for ions, molecules, and other chemical species to transport through
36 materials such as polymers,^{1, 2} metal organic frameworks, and covalent organic frameworks³ and
37 to participate in fast-kinetics electrochemical processes (*e.g.*, electrochemical reactions and
38 diffusion-limited charging/discharging processes).^{4, 5} Room temperature ionic liquids (RTIL) are
39 attractive electrolytes because of their high stability.⁶⁻⁸ Their strongly attractive intermolecular
40 forces, however, reduce their diffusion and limit their use in diffusion-controlled processes.⁹

1
2
3 Frustrated by mismatched cation and anion sizes, RTIL form a weak lattice structure, allowing
4
5
6 the ions to exist as liquids and diffuse at room temperature.¹⁰ Nevertheless, compared with aqueous
7
8
9 systems, the diffusion of RTIL is orders-of-magnitude slower. If the lattice structure is disrupted,
10
11
12 the ion diffusion properties improve.¹¹ Therefore, nanopore-induced confinement is an effective
13
14
15 method to increase ion mobility because it further weakens the lattice structure.¹² Towards
16
17
18 confining ions, both pore size and interfacial interactions play a significant role. Too strong
19
20
21 interactions between the ions and micropore surfaces lead to immobility of the former, forming a
22
23
24 fixed surface ion layer that fills the whole pore. Given slightly larger pores, which accommodate
25
26
27 more ion layers, the ions towards the center move independently of the fixed surface ion layer,
28
29
30 decoupling them from the typical ionic liquid lattice. In general, pores of larger sizes can fit more
31
32
33 ion layers in the centers, extending the effect of the disrupted ion lattice to improve the ion
34
35
36 mobility. But, if the pore size is too large, the confinement effect diminishes, and the ion diffusion
37
38
39 behavior approximates to that in the bulk. Therefore, the pore size must be small enough to disrupt
40
41
42 the lattice structure, but large enough to hold as many ions as possible to get the most benefit from
43
44
45 confinement of the ions. Moreover, the pores should be as uniform and interconnected as possible
46
47
48 to facilitate ion transport.
49
50
51
52
53
54
55
56
57
58
59
60

1
2
3
4 Block copolymer-based porous carbon fibers (PCFs) are emerging materials with unique
5
6
7 hierarchical structures that allow easy accessibility to their large internal surface areas through
8
9
10 their interconnected pores.¹³⁻¹⁵ Similar to nonporous carbon fibers, the interwoven fibers form a
11
12
13 mat with abundant inter-fiber spaces as macropores, as well as micropores intrinsically defined by
14
15
16 the inter-layer distances of graphitic carbon. The effects of the confinement remain important for
17
18
19 ionic liquid ordering.¹⁶ Unique to PCFs, however, is a unimodal interconnected mesoporous
20
21
22 network in each individual fiber, which acts as a network of channels to deliver ions to the internal
23
24
25 micropores. Ion mobility in micropores is limited due to the lack of space for ion movement
26
27
28 ([BMIM]⁺ diameter, 3.8 – 5.8 Å),¹⁷ but the mesopores provide significantly more space and allow
29
30
31 for uninhibited ion diffusion.¹⁸ The interconnected, hierarchical micro-, meso-, and macro-pores
32
33
34 within PCFs facilitate ion diffusion and show distinct ion diffusion characteristics compared to
35
36
37 other porous carbon materials.¹⁹⁻²¹ The extra pore space is especially important for electrochemical
38
39
40 applications, where ions in the fixed surface layer are mostly immobile and the space away from
41
42
43 the pore walls prevents clogging of the pores with the immobile ion layer.²² Moreover, defined by
44
45
46 the block copolymer molecular weight, the tunable mesopores offer sufficient space to hold non-
47
48
49 surface layer ions, but are tight enough to disrupt the ionic lattice structure. Therefore, we
50
51
52
53
54
55
56
57
58
59
60

1
2
3 hypothesize that the block copolymer-defined mesoporous structures will provide an exceptional
4
5
6
7 porous network for enhanced ion diffusion.
8
9



10
11
12
13
14
15
16
17
18
19
20
21
22
23
24
25
26
27
28 **Figure 1.** (a) Schematic illustration of the synthesis of PCFs from PAN-*b*-PMMA. (b) SEM image
29 of a porous carbon fiber mat. (c) Cross-sectional SEM shows the uniform mesopores within each
30 fiber. (d) TEM image illustrates internal porosity and interconnectivity of the porous network
31 inside the fibers.
32
33
34
35
36
37

38
39 To test this hypothesis, we synthesized block copolymer-based porous carbon fibers from
40 polyacrylonitrile-*block*-polymethyl methacrylate (PAN-*b*-PMMA) and investigated the diffusion
41 within. To quantify the ultimate capability of porous carbon fibers for ion diffusion, we chose a
42 RTIL system of 1-butyl-3-methylimidazolium tetrafluoroborate ([BMIM]BF₄). Self-diffusion of
43 the [BMIM] cation both in the bulk and confined in porous carbon fibers was measured using
44 quasi-elastic neutron scattering (QENS). Diffusion coefficients were compared to the literature for
45
46
47
48
49
50
51
52
53
54
55
56
57
58
59
60

1
2
3 [BMIM] confined in porous media, and the block copolymer-based porous carbon fibers showed
4
5
6
7 seven-fold faster ion diffusion than that in the bulk.
8
9

10 **2. Results and Discussion**

11
12 Porous carbon fibers were synthesized according to an established method in our previous report
13
14 **(Figure 1a and S1)**.¹³ Briefly, PMMA was synthesized via reversible addition-fragmentation
15
16 chain-transfer (RAFT) polymerization using cumyl dithiobenzoate (CDB) as the chain-transfer
17
18 agent. The purified PMMA (65.7 kDa, $\bar{M}_w/\bar{M}_n = 1.08$) was characterized by size exclusion
19
20 chromatography (SEC) with both dynamic light scattering and refractive index detectors **(Figure**
21
22 **S2)**. Then, the block copolymer was synthesized by chain extension of CDB-terminated PMMA
23
24 using acrylonitrile. The resulting PAN-*b*-PMMA (136.7 kDa, $\bar{M}_w/\bar{M}_n = 1.12$) was purified and
25
26 characterized by SEC **(Figure S2)** and ¹H NMR **(Figure S3)**. Thermogravimetric analysis (TGA)
27
28 in nitrogen showed a polymer char yield of 32% at 600 °C, and TGA simulating the fiber synthesis
29
30 conditions produced a char yield of 31% **(Figure S4)**. PAN-*b*-PMMA was electrospun into
31
32 polymer fibers, which were oxidized at 280 °C for 8 h and then pyrolyzed at 800 °C for 1 h into
33
34 porous carbon fibers. X-ray photoelectron spectroscopy (XPS) revealed the composition of the
35
36 carbon fibers, which included 10.2% N and 4.1% O **(Figure S5)**. Scanning electron microscopy
37
38 (SEM) showed the block copolymer-based porous carbon fiber mat possessed abundant
39
40 macropores in between the fibers **(Figure 1b)**. Within each fiber were interconnected mesopores,
41
42 as evidenced by the cross-sectional SEM and TEM micrographs **(Figure 1c and 1d)**. The porosity
43
44 and general interconnectivity of the pores **(Figure 1d)** suggested a large easily accessible internal
45
46 pore volume in PCFs.
47
48
49
50
51
52
53
54
55
56
57
58
59
60

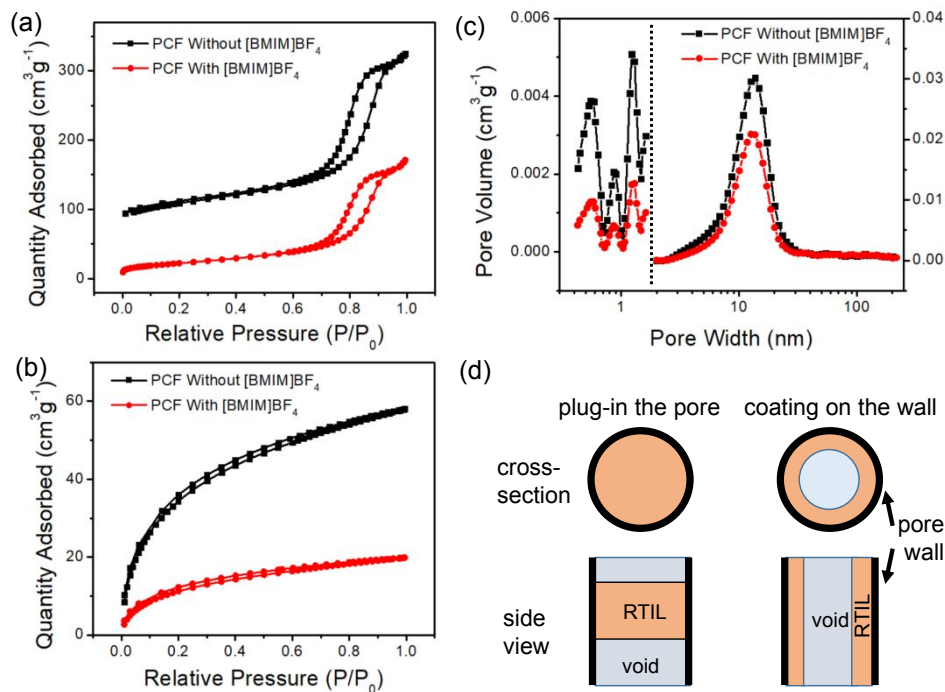


Figure 2. Representative (a) N₂ and (b) CO₂ physisorption isotherms ($n = 1$) before and after loading [BMIM]BF₄ into the porous carbon fibers. The reduced adsorbed quantities confirm the loading of the ionic liquid in the fibers. (c) Pore size distributions show that the ionic liquid occupied the pore volumes but did not change the pore sizes. (d) Physisorption suggests that [BMIM]BF₄ filled the pores as plugs (left) rather than coatings on the walls (right).

It is well known that ionic liquids behave differently in confined environments, and QENS is incapable of differentiating between the confined and unconfined ion liquids. In other words, when a porous material is fully immersed in an ionic liquid, diffusion-controlled processes are measured as a combination of diffusion outside the material (non-confined) and inside the internal pores (confined). Therefore, a high volume of confined ionic liquid is required to maximize the signal of confined ion diffusion. Porous carbon fibers have high internal volumes within their mesoporous networks and thus are ideal for QENS measurement of ion diffusion under confinement. However, it is crucial to leave macropores void and fill only the mesopores and

1
2
3 micropores with ions, properly confining the ionic liquid. Because macropores are generally too
4 large to disrupt the lattice structure of an ionic liquid significantly, any ions in the macropores
5 behave as if they are in bulk. To prepare for QENS measurement, we filled only the meso- and
6 micro-pores with the ionic liquid using vacuum infiltration^{23, 24} by suspending PCFs in a solution
7 of [BMIM]BF₄ in acetonitrile (0.015 mg/mL). The suspension was stirred for 3 h at room
8 temperature. Afterward, acetonitrile was removed by heating PCFs in an oven at 80 °C under a
9 vacuum for 12 h.

10
11
12
13
14
15
16
17
18
19
20
21
22
23
24
25
26
27
28
29
30
31
32
33
34
35
36
37
38
39
40
41
42
43
44
45
46
47
48
49
50
51
52
53
54
55
56
57
58
59
60

Physisorption tests of both N₂ at 77.4 K and CO₂ at 273.2 K (**Figure 2a and 2b**) were performed before and after loading with [BMIM]BF₄ to confirm the occupation of the meso- and micropores. After loading [BMIM]BF₄, the N₂-sorbed surface area decreased from 404 ± 1 to 76 ± 1 m²/g, as determined using the Brunauer-Emmett-Teller (BET) method. Based on non-local density functional theory (DFT), pore size distributions exhibited predominant micropore sizes of 0.55, 0.86, and 1.23 nm, as well as a mesopore peak at ~13.6 nm (**Figure 2c**). Notably, all meso- and micropore sizes remained unchanged, but the total volumes decreased by ~48.5%. The loading of the ionic liquid was not uniform throughout the pores because only about half of the pore volume was filled, but none of the neutron scattering data rely on uniformity of the ionic liquid. The neutron beam size is on the order of 10 cm² in diameter, and the neutron scattering data is only collected for neutrons that are scattered off of hydrogen atoms, negating any impact that may arise from non-uniformity. Physisorption relies on the accessibility of gas molecules to the pore surfaces. The reduced surface area and pore volume, in combination with the unchanged pore size, suggest that the ionic liquid blocked some sorption sites. The ionic liquid likely formed plugs in the pore rather than coatings on the wall (**Figure 2d**), which would lead to a reduction in the pore sizes. If the adsorbate (i.e., N₂ and CO₂) is soluble in the ionic liquid, the physisorption will give

a falsely large surface area because the adsorbate is dissolved in the liquid rather than adsorbed on the pore surfaces. Considering the low solubility of N_2 in $[BMIM]BF_4$, similar to that in $[BMIM]PF_6$,²⁵ the gas dissolution effect is unlikely to affect the N_2 results. Physisorption of CO_2 showed the same trend, and thus the effect of CO_2 solubility was also negligible. Regardless, the physisorption serves as a qualitative means for confirming the presence of the ionic liquid in the fibers.

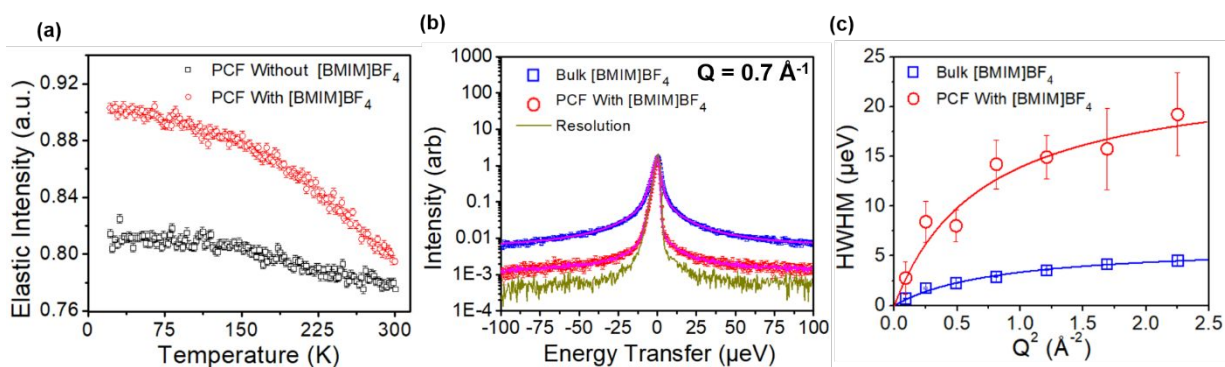


Figure 3. (a) Elastic scattering spectra of porous carbon fibers ($n = 1$) with and without $[BMIM]BF_4$. The enhanced elastic scattering intensity confirms that $[BMIM]BF_4$ was loaded into the pores. The lack of a thermal transition corresponding to the melting of $[BMIM]BF_4$ suggests the confinement of the ionic liquid in the pores. (b) Representative QENS spectra (collected for three hours) of $[BMIM]BF_4$ in the bulk and confined within the porous carbon fibers at $Q = 0.7 \text{ \AA}^{-1}$ with normalized maximum intensity ($n = 1$). (c) The extraction of HWHM at each Q allows for the determination of the Q dependence of HWHM. The Q -dependence of HWHM allows for the calculation of the diffusion coefficient of the $[BMIM]$ cation. Error bars in panel (a) represent

one standard deviation. When not visible (in panels (b) and (c)), the error bars are within the symbols. The total number of neutrons detected per sample (n) varies between 3.5×10^6 to 5.2×10^6 .

Relying on the high incoherent scattering cross-section of hydrogen atoms,²⁶ quasi-elastic neutron scattering (QENS) is the technique of choice to explore the dynamics in systems that contain hydrogen atoms.^{27, 28} Since the cation of [BMIM]BF₄ is rich in hydrogen atoms, the dynamics of the bulk and PCF-confined BMIM ions could be measured using QENS. First, temperature-dependent energy-resolved elastic scans were conducted using high flux

Table 1. Diffusion coefficient of [BMIM] cations in porous carbon fibers in comparison with those in other materials.

Systems	D_{BMIM} ($10^{-10} \text{ m}^2 \text{ s}^{-1}$)	Pore diameter (nm)	Method
Carbon-derived carbon ³²	0.52	0.8/3.1	QENS
Mesoporous carbon ³⁴	2.55	8.8	QENS
Vertically-aligned CNT ⁴⁰	0.31	4	PFG-NMR
Silicon carbide-carbon derived carbon ²³	2.32	0.8	QENS
CNT (20,20) ¹⁹	2.86	1.3	MD
CNT (40,40) ¹⁹	0.43	2.7	MD
CNT (34,0) ¹⁹	0.41	1.3	MD
Graphene Sheets ¹⁹	0.01	2.7	MD
Porous carbon fibers*	5.1	13.6	QENS

All diffusion coefficients are based on long-range diffusion at 298/300 K. CNT, carbon nanotubes; PFG-NMR, pulse field gradient nuclear magnetic resonance; and backscattering spectrometer²⁹ on the confined [BMIM]BF₄ (**Figure 3a**). The elastic intensity of the confined ionic liquid was significantly higher at 10 K compared to the bare PCF matrix, suggesting the presence of the ionic liquid in the pores (in agreement with the physisorption data).

[BMIM]BF₄ melts at 198 K, and at this temperature the elastic intensity would show a step corresponding to a thermal phase transition.^{30, 31} The absence of a step in all elastic scattering spectra collected for [BMIM]BF₄ in the fibers, however, confirmed the confinement of [BMIM]BF₄ within the pores and the disruption of the ionic liquid's lattice structure.³² Additionally, the absence of water and acetonitrile in [BMIM]BF₄ inside the pores was confirmed by the lack of any significant step at 273 K (water's freezing point) or 228 K (acetonitrile's freezing point). **Figure 3 (main panel)** shows representative quasi-elastic spectra measured using backscattering silicon spectrometer³³ and the corresponding model fits (See SI for details) of the bulk and confined [BMIM]BF₄, together with the instrument resolution. Even though the spectrum collected from the bulk [BMIM]BF₄ appeared to exhibit more pronounced QENS broadening than that for the confined [BMIM]BF₄, the data analysis (using Eq. 1, SI) demonstrates that the mobile ions in the confined ionic liquid (those that contributed to the QENS signal rather than the elastic line) gave rise to a relatively broader signal. In other words, while the overall QENS intensity for the PCFs with [BMIM]BF₄ was lower due to immobilized ions that contributed only to the elastic scattering, those that remained mobile exhibited higher diffusivity than the ions in the bulk [BMIM]BF₄ despite its overall higher QENS intensity. The half-width at half-maximum (HWHM) of the slow components of the bulk and confined [BMIM]BF₄ (**Figure 3b**) showed a non-linear dependence on Q^2 , which corresponded to a long-range translational mobility of the ions.^{34, 35} Therefore, the translational diffusion coefficient (D) of the cation in the bulk liquid was determined using a jump diffusion model (diffusion with a relaxation time), giving a value of $(0.73 \pm 0.06) \times 10^{-10} \text{ m}^2\text{s}^{-1}$, in agreement with similar systems in a previous report.³⁴ The diffusion dynamics of the confined cation were found to be non-homogeneous, i.e., non-exponential, requiring the introduction of an exponent $\alpha(Q) = 0.5$ (a typical value used for other small molecule glass

1
2
3 formers)^{36, 37} to fit the data using a Cole-Cole distribution function (see SI for detail). This
4
5 functional form has been employed successfully in many confined systems.^{38, 39} For the confined
6
7 [BMIM] cation, the diffusion coefficient value was determined to be $(5.1 \pm 1.1) \times 10^{-10} \text{ m}^2 \text{ s}^{-1}$,
8
9 about ~ 7 times greater than that of the unconfined bulk.
10

11
12 Although this enhanced diffusion behavior of the confined fluid has been witnessed in other
13
14 materials,¹⁴ the amount of enhancement is unprecedented. Compared to all available materials to
15
16 date, the porous carbon fibers show the largest increase in diffusion coefficient for the [BMIM]
17
18 cation (**Table 1**), likely owing to a few features of PCFs.⁴⁰ Our porous carbon fibers are hydrophilic
19
20 due to the high content of surface N and O heteroatoms, similar to our previous reports.^{20, 41} The
21
22 heteroatom content of the PCFs contrasts with the rest of the works cited in **Table 1**. Due to the
23
24 hydrophilic PCFs, ions stabilize along the surface of the pores. The stabilized surface-layer ions
25
26 decouple from the ions in the diffuse layer and prevent effective long-range ion packing. Owing
27
28 to reduced IL packing, the diffusion layers within the mesopores exhibit lower viscosity and
29
30 friction. The balance of pore volume and packed layers becomes imperative for enhanced diffusion
31
32 within the carbon matrix.⁴² The mesopore size allowed for a significant amount of confined ionic
33
34 liquid to exist in the diffuse-layer rather than the adsorbed-layer. The lack of a transition in the
35
36 elastic scan across the examined temperature range (**Figure 3a**) indicated that the disrupted lattice
37
38 structure extends across the whole pore, frustrating the ion packing. Thus, ions in the diffuse layer
39
40 do not freeze between 10 K and 300 K, *despite the typical freezing point of [BMIM]BF₄ being 198*
41
42 *K*. The disruption of the lattice, in combination with the reduced friction between the adsorbed
43
44 ions and the confined diffuse-layer ions, leads to the exceptionally high diffusion coefficient. Our
45
46 results match the observations of Dyatkin *et al.*,²³ where the ions inside 0.8-nm micropores were
47
48 immobile and the high diffusion coefficient was attributed to the inner ion layers inside mesopores.
49
50
51
52
53
54
55
56
57
58
59
60

1
2
3 Ghoufi *et al.* also found a large increase in diffusion of the [BMIM] cation in 1.3 nm diameter
4 pores of (20,20) carbon nanotubes (CNTs), owing to a small friction.¹⁹ Additionally, Ohba *et al.*
5
6 found a reduction in ionic liquid viscosity within CNTs and the ions revealed ordered coordination
7
8 with CNT walls when the micropore diameters were 0.63, 0.86, 1.28, and 1.73 nm.⁴³ Similarly,
9
10 the ion diffusion in PCFs also showed a positive correlation with micropore sizes of 0.55, 0.86,
11
12 and 1.23 nm (**Figure 2c**). Ionic liquid diffusion in mesoporous carbon for supercapacitors was also
13
14 studied by Liu *et al.*, who found a juxtaposition between pore size and electrochemical
15
16 performance limited by ion diffusion.⁴⁴ The fastest ion diffusion in mesoporous carbon was found
17
18 when mesopore sizes were 13.9 nm for cations with a size of 7.6 Å, in agreement with the favorable
19
20 mesopore size of 13.6 nm in PCFs herein.⁴⁴ In addition, the surface interactions resulting from
21
22 heteroatoms further improved the ion diffusion characteristics, in consistence with the previous
23
24 finding that the heteroatomic species of N-X and O/O-H provide a layered surface for aligned
25
26 cations to facilitate rapid ionic diffusion.^{45, 46}

33 **3. Conclusions**

34 In summary, advanced QENS measurements show that the block copolymer-based porous carbon
35
36 fibers have exceptional ion diffusion properties. The confined ions exhibit a seven-fold increase
37
38 in the diffusion coefficient. Attachment of the cations to the pore wall (which are not mobile within
39
40 the sensitivity of the instrument) contributes to the elastic incoherent scattering fraction, which, in
41
42 turn, can be related to the electrochemical capacitance of porous materials. The fast diffusivity of
43
44 the cations away from the wall could contribute to the high-rate capability of the porous carbon
45
46 fibers for use in supercapacitors, as well as fast charging/discharging in batteries. The exceptional
47
48 ion diffusion also holds great promise for fast mass transport in electrochemical catalysis. Lastly,
49
50 tunability in PCF properties based on the initial block copolymer offers opportunities to control
51
52 hydrophilicity, pore size, and other characteristics to further adjust the confinement effect.
53
54
55
56
57
58
59
60

1
2
3 Therefore, the block copolymer-based porous carbon fibers represent an outstanding platform
4 material for electrochemical applications.
5
6

7 8 **4. Experimental Section** 9

10 11 **4.1 Fiber Characterization** 12

13
14 A Micromeritics-3Flex pore analyzer was used to determine the surface areas and porosities of the
15 porous carbon fibers. A sample of ~50 mg fibers was placed into a physisorption tube and degassed
16 at 300 °C for 10 h to remove oxygen and any adsorbed volatile species. The mass of the fibers was
17 recorded by subtracting post-degas mass from the mass of the empty tube. CO₂-sorption tests were
18 carried out using CO₂ and dipping the physisorption tube into a Dewar containing ice water (273
19 K). N₂-sorption tests were carried out using N₂ and dipping the physisorption tube into a Dewar
20 containing liquid nitrogen (77 K). One sample (n = 1) of PCF with and without ionic liquid was
21 used for both N₂ and CO₂ physisorption tests.
22
23
24
25
26
27
28
29
30
31
32
33
34
35

36 Fiber morphology was characterized using electron microscopy imaging. Scanning electron
37 microscopy (SEM, LEO Zeiss 1550) images were taken using an accelerating voltage of 3 kV and
38 a working distance of 2.9 mm (Figures 1b and 1c). To prepare for transmission electron
39 microscopy (TEM), PCFs were dispersed in deionized water by ultrasonication. A drop of the
40 suspension was then spread on a carbon-coated copper TEM grid, followed by drying on a hot
41 plate at 60 °C for 30 min. TEM images were then collected on a probe-corrected transmission
42 electron microscope (FEI ChemiSTEM 80-200) operating at 200 kV (Figure 1d).
43
44
45
46
47
48
49
50
51
52
53

54 **4.2 Vacuum Infiltration of [BMIM]BF₄ into Pores** 55 56 57 58 59 60

1
2
3
4 Porous carbon fibers were suspended in a solution of [BMIM]BF₄ in acetonitrile (0.015 mg/mL).
5
6 The suspension was stirred for 3 h in a glovebox with an argon atmosphere. Afterward, the
7
8 suspension was transferred to a vacuum oven to remove acetonitrile at 80 °C, leaving behind the
9
10 [BMIM]BF₄ inside the pores of porous carbon fibers.
11
12

13 14 **4.3 Neutron Scattering Experiments** 15

16
17
18 Neutron scattering experiments were performed using two neutron backscattering spectrometers,
19
20 with the sample temperature controlled using closed-cycle refrigerators. Fixed window scans of
21
22 the elastic scattering intensity were performed using the High Flux Backscattering Spectrometer
23
24 (HFBS)²⁹ at NIST Center for Neutron Research in Gaithersburg, MD. HFBS has an energy
25
26 resolution of 0.8 μeV (full width at half maximum, FWHM). The instrument covers a momentum
27
28 transfer vector (Q) range of 0.25 Å⁻¹ to 1.74 Å⁻¹ and an energy transfer range of ± 16 μeV. Elastic
29
30 intensity spectra from the 0.25 mm thick samples, which were loaded in flat plate aluminum
31
32 sample holders, were collected with a heating rate of 1 K/min. The data were reduced using DAVE
33
34 software⁴⁷ available at NIST-NCNR.
35
36
37
38
39
40

41
42 Quasielastic neutron scattering (QENS) measurements of both the bulk and confined ionic
43
44 liquid were carried out using the Backscattering Silicon Spectrometer (BASIS)³³ at the Spallation
45
46 Neutron Source in the Oak Ridge National Laboratory, Oak Ridge, TN. The instrument was
47
48 operated at its standard configuration, which provides an energy resolution of 3.7 μeV (FWHM),
49
50 using a bandwidth of incoming neutrons centered at 6.4 Å and covering an energy range of ± 100
51
52 μeV. This setup of the instrument spans a Q range of 0.2 Å⁻¹ to 2.0 Å⁻¹. QENS spectra were
53
54
55
56
57
58
59
60

1
2
3 collected at 300 K along with the sample-specific instrument resolution at 20 K. Mantid software⁴⁸
4
5 was used for the data reduction. The analysis of the data was performed using the DAVE package.
6
7
8 The errors on the parameters after QENS peak fitting are obtained from the chi-squared minimization and
9
10 represent one standard deviation. The number of samples was n=1 for all compositions (one PCF
11
12 sample with ionic liquid, one PCF sample without ionic liquid, and one sample of pure ionic liquid.
13
14
15 The total number of neutrons detected per sample varies between 3.5×10^6 and 5.2×10^6 .
16
17
18

19 ASSOCIATED CONTENT

20
21 **Supporting Information.** This material is available free of charge via the Internet at
22
23 <http://pubs.acs.org>. SEC and TGA traces; ¹H NMR and XPS spectra.
24
25
26

27 Notes

28
29 The authors declare no competing financial interest.
30
31
32

33 AUTHOR INFORMATION

34 Corresponding Authors

35 Guoliang Liu - Department of Chemistry, Virginia Tech, Blacksburg, VA 24061, United States;
36 Macromolecules Innovation Institute, Virginia Tech, Blacksburg, VA 24061, United States;
37 orcid.org/0000-0002-6778-0625; Email: gliu1@vt.edu
38
39

40 Naresh Osti - Neutron Scattering Division, Oak Ridge National Laboratory, PO BOX 2008
41 MS6455, Oak Ridge, TN 37831, United States; orcid.org/0000-0002-0213-2299; Email:
42 ostinc@ornl.gov
43
44

45 Authors

46 John Elliott - Department of Chemistry, Virginia Tech, Blacksburg, VA 24061, United States;
47 orcid.org/0000-0003-4560-8493; Email: johnelliott@vt.edu
48
49

50 Madhusudan Tyagi - NIST Center for Neutron Research, National Institute of Standards and
51 Technology, Gaithersburg, Maryland 20899, United States; Department of Materials Science,
52 University of Maryland, College Park, Maryland 20742, United States; orcid.org/0000-0002-7378-0701;
53 Email: madhusudan.tyagi@nist.gov
54
55
56
57
58
59
60

1
2
3 Eugene Mamontov - Neutron Scattering Division, Oak Ridge National Laboratory, PO BOX
4 2008 MS6455, Oak Ridge, TN 37831, United States; orcid.org/0000-0002-5684-2675; Email:
5 mamontove@ornl.gov
6

7
8 Lifeng Liu - International Iberian Nanotechnology Laboratory (INL), Avenida Mestre José
9 Veiga, 4715-330 Braga, Portugal; orcid.org/0000-0003-2732-7399; Email: Lifeng.Liu@inl.int
10

11 Joel Serrano - Department of Chemistry, Virginia Tech, Blacksburg, VA 24061, United States;
12 orcid.org/0000-0001-7204-7455; Email: sjoel5@vt.edu
13

14
15 Ke Cao - Macromolecules Innovation Institute, Virginia Tech, Blacksburg, VA 24061, United
16 States; orcid.org/0000-0001-7204-7455; Email: kecaogod@vt.edu
17

18 19 20 ACKNOWLEDGMENT

21
22
23 This article contains studies supported by the National Science Foundation under Grant No. DMR-
24 1752611 through the CAREER award and the American Chemical Society Petroleum Research
25 Foundation Doctoral New Investigator Award. Work at ORNL's Spallation Neutron Source was
26 sponsored by the Scientific User Facilities Division, Office of Basic Energy Sciences, U.S.
27 Department of Energy. Oak Ridge National Laboratory is managed by UT-Battelle, LLC, for U.S.
28 DOE under Contract No. DEAC05-00OR22725. Experiments on HFBS at NIST Center for
29 Neutron Research (NCNR) were supported in part by the National Science Foundation under
30 Agreement No. DMR-2010792. Certain commercial material suppliers are identified in this paper
31 to foster understanding. Such identification does not imply recommendation or endorsement by
32 the National Institute of Standards and Technology, nor does it imply that the materials or
33 equipment identified are necessarily the best available for the purpose.
34
35
36
37
38
39
40
41
42
43
44
45
46
47
48

49 REFERENCES

- 50
51 1. Kim, S.; Ju, M.; Lee, J.; Hwang, J.; Lee, J., Polymer Interfacial Self-Assembly Guided
52 Two-Dimensional Engineering of Hierarchically Porous Carbon Nanosheets. *J Am Chem*
53 *Soc* **2020**, *142*, 9250-9257.
54
55
56
57
58
59
60

2. Rouhani, F.; Rafizadeh-Masuleh, F.; Morsali, A., Highly Electroconductive Metal-Organic Framework: Tunable by Metal Ion Sorption Quantity. *J Am Chem Soc* **2019**, *141*, 11173-11182.
3. Yu, M.; Chandrasekhar, N.; Raghupathy, R. K. M.; Ly, K. H.; Zhang, H.; Dmitrieva, E.; Liang, C.; Lu, X.; Kuhne, T. D.; Mirhosseini, H.; Weidinger, I. M.; Feng, X., A High-Rate Two-Dimensional Polyarylimide Covalent Organic Framework Anode for Aqueous Zn-Ion Energy Storage Devices. *J Am Chem Soc* **2020**, *142*, 19570-19578.
4. Salim, N. V.; Mateti, S.; Cizek, P.; Hameed, N.; Parameswaranpillai, J.; Fox, B., Large, Mesoporous Carbon Nanoparticles with Tunable Architectures for Energy Storage. *ACS Applied Nano Materials* **2019**, *2*, 1727-1736.
5. Zhong, M.; Kim, E. K.; McGann, J. P.; Chun, S. E.; Whitacre, J. F.; Jaroniec, M.; Matyjaszewski, K.; Kowalewski, T., Electrochemically Active Nitrogen-Enriched Nanocarbons with Well-Defined Morphology Synthesized by Pyrolysis of Self-Assembled Block Copolymer. *J Am Chem Soc* **2012**, *134*, 14846-57.
6. Rogers, R. D.; Seddon, K. R., Ionic Liquids--Solvents of the Future? *Science* **2003**, *302*, 792-793.
7. Wasserscheid, P., Chemistry: Volatile Times for Ionic Liquids. *Nature* **2006**, *439*, 797.
8. Liang, Y.; Liu, H.; Li, Z.; Fu, R.; Wu, D., In Situ Polydopamine Coating-Directed Synthesis of Nitrogen-Doped Ordered Nanoporous Carbons with Superior Performance in Supercapacitors. *Journal of Materials Chemistry A* **2013**, *1*, 15207.
9. Lin, R.; Huang, P.; Ségalini, J.; Largeot, C.; Taberna, P. L.; Chmiola, J.; Gogotsi, Y.; Simon, P., Solvent Effect on the Ion Adsorption from Ionic Liquid Electrolyte into Sub-Nanometer Carbon Pores. *Electrochimica Acta* **2009**, *54*, 7025-7032.
10. Hayes, R.; Warr, G. G.; Atkin, R., Structure and Nanostructure in Ionic Liquids. *Chem Rev* **2015**, *115*, 6357-426.
11. Rajput, N. N.; Monk, J.; Singh, R.; Hung, F. R., On the Influence of Pore Size and Pore Loading on Structural and Dynamical Heterogeneities of an Ionic Liquid Confined in a Slit Nanopore. *J Phys Chem C* **2012**, *116*, 5169-5181.
12. Singh, M. P.; Singh, R. K.; Chandra, S., Ionic Liquids Confined in Porous Matrices: Physicochemical Properties and Applications. *Prog Mater Sci* **2014**, *64*, 73-120.
13. Zhou, Z.; Liu, T.; Khan, A.; Liu, G., Block Copolymer-Based Porous Carbon Fibers. *Sci. Adv.* **2019**, *5*, eaau6852.
14. Liu, T.; Serrano, J.; Elliott, J.; Yang, X.; Cathcart, W.; Wang, Z.; He, Z.; Liu, G., Exceptional Capacitive Deionization Rate and Capacity by Block Copolymer-Based Porous Carbon Fibers. *Sci Adv* **2020**, *6*, eaaz0906.
15. Liu, T.; Liu, G., Block Copolymer-Based Porous Carbons for Supercapacitors. *J Mater Chem A* **2019**, *7*, 23476-23488.
16. Futamura, R.; Iiyama, T.; Takasaki, Y.; Gogotsi, Y.; Biggs, M. J.; Salanne, M.; Segalini, J.; Simon, P.; Kaneko, K., Partial Breaking of the Coulombic Ordering of Ionic Liquids Confined in Carbon Nanopores. *Nat Mater* **2017**, *16*, 1225-1232.
17. Gutiérrez, A.; Atilhan, M.; Alcalde, R.; Trenzado, J. L.; Aparicio, S., Insights on the Mixtures of Imidazolium Based Ionic Liquids with Molecular Solvents. *Journal of Molecular Liquids* **2018**, *255*, 199-207.
18. Peng, J.; Zhang, W.; Yu, P.; Pang, H.; Zheng, M.; Dong, H.; Hu, H.; Xiao, Y.; Liu, Y.; Liang, Y., Improved Ion-Diffusion Performance by Engineering an Ordered

- Mesoporous Shell in Hollow Carbon Nanospheres. *Chem Commun (Camb)* **2020**, *56*, 2467-2470.
19. Ghoufi, A.; Szymczyk, A.; Malfreyt, P., Ultrafast Diffusion of Ionic Liquids Confined in Carbon Nanotubes. *Sci Rep* **2016**, *6*, 28518.
20. Serrano, J. M.; Liu, T.; Khan, A. U.; Botset, B.; Stovall, B. J.; Xu, Z.; Guo, D.; Cao, K.; Hao, X.; Cheng, S.; Liu, G., Composition Design of Block Copolymers for Porous Carbon Fibers. *Chem Mater* **2019**, *31*, 8898-8907.
21. Miao, L.; Duan, H.; Liu, M.; Lu, W.; Zhu, D.; Chen, T.; Li, L.; Gan, L., Poly(Ionic Liquid)-Derived, N, S-Codoped Ultramicroporous Carbon Nanoparticles for Supercapacitors. *Chemical Engineering Journal* **2017**, *317*, 651-659.
22. Kondrat, S.; Wu, P.; Qiao, R.; Kornyshev, A. A., Accelerating Charging Dynamics in Subnanometre Pores. *Nat Mater* **2014**, *13*, 387-93.
23. Dyatkin, B.; Osti, N. C.; Gallegos, A.; Zhang, Y.; Mamontov, E.; Cummings, P. T.; Wu, J.; Gogotsi, Y., Electrolyte Cation Length Influences Electrosorption and Dynamics in Porous Carbon Supercapacitors. *Electrochim Acta* **2018**, *283*, 882-893.
24. Dyatkin, B.; Mamontov, E.; Cook, K. M.; Gogotsi, Y., Capacitance, Charge Dynamics, and Electrolyte Surface Interactions in Functionalized Carbide Derived Carbon Electrodes. *Prog. Nat. Sci.* **2015**, *25*, 631-641.
25. Anthony, J. L.; Maginn, E. J.; Brennecke, J. F., Solubilities and Thermodynamic Properties of Gases in the Ionic Liquid 1-N-Butyl-3-Methylimidazolium Hexafluorophosphate. *J Phys Chem B* **2002**, *106*, 7315-7320.
26. Bee, M., *Quasielastic Neutron Scattering: Principles and Applications in Solid State Chemistry, Biology, and Materials Science*. Adam Hilger, Bristol: 1998; p 28.
27. Osti, N. C.; Mamontov, E., Microscopic Dynamics in Room-Temperature Ionic Liquids Confined in Materials for Supercapacitor Applications. *Sustain Energ Fuels* **2020**, *4*, 1554-1576.
28. Osti, N. C.; Cote, A.; Mamontov, E.; Ramirez-Cuesta, A.; Wesolowski, D. J.; Diallo, S. O., Characteristic Features of Water Dynamics in Restricted Geometries Investigated with Quasi-Elastic Neutron Scattering. *Chem Phys* **2016**, *465*, 1-8.
29. Meyer, A.; Dimeo, R.; Gehring, P.; Neumann, D., The High-Flux Backscattering Spectrometer at the Nist Center for Neutron Research. *Review of Scientific Instruments* **2003**, *74*, 2759-2777.
30. Mamontov, E.; Luo, H. M.; Dai, S., Proton Dynamics in N,N,N',N'-Tetramethylguanidinium Bis(Perfluoroethylsulfonyl)Imide Protic Ionic Liquid Probed by Quasielastic Neutron Scattering. *J Phys Chem B* **2009**, *113*, 159-169.
31. Prisk, T. R.; Tyagi, M.; Sokol, P. E., Dynamics of Small-Molecule Glass Formers Confined in Nanopores. *J Chem Phys* **2011**, *134*, 114506.
32. Osti, N. C.; Dyatkin, B.; Thompson, M. W.; Tiet, F.; Zhang, P. F.; Dai, S.; Tyagi, M.; Cummings, P. T.; Gogotsi, Y.; Wesolowski, D. J.; Mamontov, E., Influence of Humidity on Performance and Microscopic Dynamics of an Ionic Liquid in Supercapacitor. *Phys Rev Mater* **2017**, *1*, 035402.
33. Mamontov, E.; Herwig, K. W., A Time-of-Flight Backscattering Spectrometer at the Spallation Neutron Source, Basis. *Review of Scientific Instruments* **2011**, *82*, 085109.
34. Chathoth, S. M.; Mamontov, E.; Dai, S.; Wang, X.; Fulvio, P. F.; Wesolowski, D. J., Fast Diffusion in a Room Temperature Ionic Liquid Confined in Mesoporous Carbon. *EPL (Europhysics Letters)* **2012**, *97*, 66004.

- 1
2
3 35. Chathoth, S. M.; Mamontov, E.; Fulvio, P. F.; Wang, X.; Baker, G. A.; Dai, S.;
4 Wesolowski, D. J., An Unusual Slowdown of Fast Diffusion in a Room Temperature
5 Ionic Liquid Confined in Mesoporous Carbon. *EPL (Europhysics Letters)* **2013**, *102*,
6 16004.
7
8 36. Borjesson, L.; Elmroth, M.; Torell, L. M., Neutron and Light-Scattering Study of
9 Relaxation Dynamics in a Glass-Forming Fragile Molecular Liquid. *Chem Phys* **1990**,
10 *149*, 209-220.
11 37. Tyagi, M.; Arbe, A.; Alvarez, F.; Colmenero, J.; Gonzalez, M., Short-Range Order and
12 Collective Dynamics of Poly(Vinyl Acetate): A Combined Study by Neutron Scattering
13 and Molecular Dynamics Simulations. *J Chem Phys* **2008**, *129*, 224903-14.
14 38. Dyatkin, B.; Osti, N. C.; Zhang, Y.; Wang, H.-W.; Mamontov, E.; Heller, W. T.;
15 Zhang, P.; Rother, G.; Cummings, P. T.; Wesolowski, D. J.; Gogotsi, Y., Ionic Liquid
16 Structure, Dynamics, and Electrosorption in Carbon Electrodes with Bimodal Pores and
17 Heterogeneous Surfaces. *Carbon* **2018**, *129*, 104-118.
18 39. Osti, N. C.; Dyatkin, B.; Gallegos, A.; Voneshen, D.; Keum, J. K.; Littrell, K.; Zhang,
19 P. F.; Dai, S.; Wu, J. Z.; Gogotsi, Y.; Mamontov, E., Cation Molecular Structure
20 Affects Mobility and Transport of Electrolytes in Porous Carbons. *J Electrochem Soc*
21 **2019**, *166*, A507-A514.
22 40. Berrod, Q.; Ferdeghini, F.; Judeinstein, P.; Genevaz, N.; Ramos, R.; Fournier, A.;
23 Dijon, J.; Ollivier, J.; Rols, S.; Yu, D.; Mole, R. A.; Zanotti, J. M., Enhanced Ionic
24 Liquid Mobility Induced by Confinement in 1d Cnt Membranes. *Nanoscale* **2016**, *8*,
25 7845-8.
26 41. Zhou, Z.; Liu, T.; Khan, A. U.; Liu, G., Controlling the Physical and Electrochemical
27 Properties of Block Copolymer-Based Porous Carbon Fibers by Pyrolysis Temperature.
28 *Mol Syst* **2020**, *5*, 153-165.
29 42. Liu, T.; Zhang, F.; Song, Y.; Li, Y., Revitalizing Carbon Supercapacitor Electrodes with
30 Hierarchical Porous Structures. *Journal of Materials Chemistry A* **2017**, *5*, 17705-17733.
31 43. Ohba, T.; Chaban, V. V., A Highly Viscous Imidazolium Ionic Liquid inside Carbon
32 Nanotubes. *J Phys Chem B* **2014**, *118*, 6234-40.
33 44. Liu, Y.; Zhang, H.; Song, H.; Noonan, O.; Liang, C.; Huang, X.; Yu, C., Single-
34 Layered Mesoporous Carbon Sandwiched Graphene Nanosheets for High Performance
35 Ionic Liquid Supercapacitors. *The Journal of Physical Chemistry C* **2017**, *121*, 23947-
36 23954.
37 45. Choi, W.; Ulissi, Z. W.; Shimizu, S. F.; Bellisario, D. O.; Ellison, M. D.; Strano, M. S.,
38 Diameter-Dependent Ion Transport through the Interior of Isolated Single-Walled Carbon
39 Nanotubes. *Nat Commun* **2013**, *4*, 2397.
40 46. Elverfeldt, C. P.; Lee, Y. J.; Froba, M., Selective Control of Ion Transport by
41 Nanoconfinement: Ionic Liquid in Mesoporous Resorcinol-Formaldehyde Monolith. *ACS*
42 *Appl Mater Interfaces* **2019**, *11*, 24423-24434.
43 47. Azuah, R. T.; Kneller, L. R.; Qiu, Y. M.; Tregenna-Piggott, P. L. W.; Brown, C. M.;
44 Copley, J. R. D.; Dimeo, R. M., Dave: A Comprehensive Software Suite for the
45 Reduction, Visualization, and Analysis of Low Energy Neutron Spectroscopic Data.
46 *Journal of Research of the National Institute of Standards and Technology* **2009**, *114*,
47 341-358.
48 48. Arnold, O.; Bilheux, J. C.; Borreguero, J. M.; Buts, A.; Campbell, S. I.; Chapon, L.;
49 Doucet, M.; Draper, N.; Leal, R. F.; Gigg, M. A.; Lynch, V. E.; Markvardsen, A.;
50
51
52
53
54
55
56
57
58
59
60

1
2
3 Mikkelsen, D. J.; Mikkelsen, R. L.; Miller, R.; Palmen, K.; Parker, P.; Passos, G.;
4 Perring, T. G.; Peterson, P. F.; Ren, S.; Reuter, M. A.; Sayici, A. T.; Taylor, J. W.;
5 Taylor, R. J.; Tolchenoy, R.; Zhou, W.; Zikoysky, J., Mantid-Data Analysis and
6 Visualization Package for Neutron Scattering and Mu Sr Experiments. *Nuclear*
7 *Instruments & Methods in Physics Research Section a-Accelerators Spectrometers*
8 *Detectors and Associated Equipment* **2014**, 764, 156-166.
9
10
11
12
13
14

15 TOC GRAPHICS

